Van Allen Belt Punctures and their Correlation with Solar Wind, Geomagnetic Activity and ULF Waves

J. Joseph[1], A. N. Jaynes[1], D. N. Baker[2], X. Li[2], and S. G. Kanekal[3]

[1]Department of Physics and Astronomy, University of Iowa, IA, USA

[2]Laboratory for Atmospheric and Space Science, University of Colorado Boulder, CO, USA

[3]NASA Goddard Space Flight Center, MD, USA

Corresponding author: Jayasri Joseph (jayasri-joseph@uiowa.edu)

Key Points:

- Puncture events have very little correlation with the strength of the geomagnetic disturbances.
- Puncture events occur following high-speed solar wind or ICMEs depending on the phase of the solar cycle.
- ULF wave activity can predict at least 75% of the puncture events.

Abstract

We investigate the rare events of sudden appearances of relativistic electrons (>700 keV), which are normally confined to the Van Allen belts, in the slot region. The frequency of occurrence of these events are on average 1-2 per year. To cope with the scarcity of events, in this study we examine 21 years of trapped relativistic electron fluxes available from the POES and MetOp Space Environment Monitor (SEM-2). Our statistical analysis show that these events can occur even during moderate geomagnetic activity. Occurrence of these events correlates with high speed solar winds or ICMEs depending on the phase of the solar cycle. Most importantly, we show that ULF wave activity plays a significant role in causing these events and the events could be predicted in 75% of the cases.

1 Introduction

The Earth is protected against harsh energetic particles from space by the Van Allen radiation belts – regions that contain charged particles captured by the Earth's magnetic field. The Van Allen belts can be a source of highly energetic electrons (Kanekal et al., 2001) that increase and decrease on varying timescales. Long-term observations of the outer radiation belt reveals that on rare occasions there are punctures, which are defined in this study as a sudden enhancement of relativistic (>700 keV) electron flux by greater than three orders of magnitude in the slot region (2<L<2.8) within a day. These events are of importance in understanding the physics of the radiation belts and the evolution of electron fluxes during geomagnetic disturbances.

Relativistic and ultra-relativistic electrons in the slot region, where important space assets including GPS satellites are located, pose a natural hazard. Many studies using data from numerous satellites were conducted in the past to understand and predict the energetic particle appearances in the slot region. Three decades ago, the Combined Release and Radiation Effects Satellite (CRRES) observed simultaneous injections of MeV protons and electrons at 2<L<3 after a solar flare event as reported by Blake et al. (1992). This event created a third radiation belt due to the interplanetary shock impact and was reproduced in a simulation by Li et al. (1993). A model to forecast the relativistic electron fluxes in real time inside geosynchronous orbit and down to L = 2.5 in extreme storm events was also developed by Li et al. (2009). Zhao and Li (2013) analyzed ten years of SAMPEX 2–6 MeV electron flux data and found 23 injection events during which the electron flux at L = 2.5 increased by at least one order of magnitude. They also noted a correlation of injection events with IMF magnitude, IMF Bz, solar wind electric field, and solar wind speed. However, there are some disagreements about the detection of electrons with energies above 1 MeV in the slot region by the SAMPEX instrument (Selesnick, 2015). As electron flux enhancement is a prerequisite for the appearance of electrons in the slot region, many studies focused on electron activities inside the radiation belt. Kanekal (2006) examined the SAMPEX and Polar data and showed that the electron energization in the radiation belt could be either due to radial diffusion or wave-particle interactions. He also showed a correlation between the energization processes and the phases of the solar cycle. Rodger et al. (2010) studied 10 years of measurements of trapped and precipitating electrons from the POES Satellites and showed that the relativistic (>800 keV) electron enhancement in the belt lags by approximately one week relative to the low energy (~30 keV) electron enhancement. Many observations of the outer radiation belt indicated a nominal energy

dependent barrier isolating the slot region from the belt. The Relativistic Electron Proton Telescope (REPT) instrument onboard the Van Allen Probes mission detected a very sharp inner boundary of the outer radiation belt for the ultra-relativistic electrons (>2 MeV) at L= 2.8, which was reported by Baker et al. (2014) and referred to as 'impenetrable barrier'. This barrier becomes semi-rigid for low-energy electrons and a rigidity profile of the barrier was recorded by Turner et al. (2016). They studied electron fluxes of the radiation belts from Van Allen Probes data during 2012–2014 and found that sudden particle enhancements (SPELLS) at L < 2.8 are common for low-energy electrons but decreases exponentially with increasing electron energies greater than 100 keV. Relativistic punctures, which involve electrons with energies >700keV, are relatively rare phenomena.

Along with the observation and cataloging of the enhancements of the relativistic and ultra-relativistic electrons in the slot region, various studies were conducted to determine the underlying cause of the sudden appearance of these electrons in the radiation belt. Baker et al. (1998) and Rostoker et al. (1998) each suggested that a relativistic electron flux enhancement needs both seed electron population of energy 100 – 200 keV and powerful occurrence of ULF waves in the PC 4 –5 frequency range. Rostoker et al. (1998) also noted that ULF waves tend to accompany high speed solar wind streams. Liu et al. (1999) proved this observation of acceleration of electrons by large scale ULF wave theoretically. O'Brien et al. (2001) performed an extensive statistical analysis of energetic electron enhancements using data from GOES and LANL. Their superposed analysis revealed that along with the solar wind velocity, the ULF power recorded by ground stations are an indicator of energetic electron enhancements. A data base of ULF wave activity indices, which were derived from the world-wide array of magnetic data from the ground stations and from the three-component magnetometer data from the geostationary GOES spacecrafts, were cataloged by Philipenko et al. (2017).

As puncture events are a relatively rare phenomena, data samples over many years, preferably from a single instrument, are needed to carry out a meaningful statistical analysis and determine possible prediction strategies. Moreover, to see any correlation of these events with solar cycle variations, observations spanning at least a couple of solar cycles is required. Here we use the Space Environment Monitor (SEM-2) instruments on the Polar Orbiting POES and MetOp satellites to obtain a continuous data set for puncture events spanning the last 21 years. SEM-2 instruments are not designed to measure relativistic electrons, although we can utilize proton channels contaminated by high-energy electrons. We trade off the inaccuracy in the energy range measurement for the long periods of continuous observations. Low altitude polar orbits also have the added advantage of sampling the belts frequently and recording events with a greater temporal accuracy than equatorially orbiting satellites.

In this work, we firstly identify the puncture events and perform a statistical analysis involving various solar wind parameters and indices during different phases of solar cycles. We show that the roles played by solar wind to cause a puncture is different during the rising and falling phases of the solar cycles. Secondly, we analyzed the correlation of puncture events with the ULF wave activity. We show that 75% of the observed puncture events over the last 21 years match with predicted events using an algorithm based on the ULF wave activity indices.

2 Instrument

In this study we use particle measurements by the SEM-2 instrument package onboard the POES and MetOp satellites. These satellites traverse Sun-synchronous orbits at an altitude of ~800–850 km. SEM-2 is a multichannel, charged-particle spectrometer that measures the population of electrons and protons in the Earth's radiation belts and is used to observe particle fluxes variations resulting from solar and extrasolar activity. There are two orthogonal channels that measure electron fluxes at 0° and 90°. The 0° measurements come from detectors that are mounted on the three-axis stabilized platform pointing outward and parallel to the Earth-center-to-satellite radial vector. The 90° measurements come from the detectors that are mounted approximately perpendicular to the 0° detectors. Table 1 lists the detector channels that respond to electrons of various energy ranges. From Table 1, it can be noted that the P6-detector, which is designed to measure >6.9 MeV protons, also responds to electrons, with energies starting from 700 keV. In this work, we use the P6-90 channel as a proxy for the trapped relativistic electron measurements of the Van Allen belt.

Table 1. List of SEM-2 energy channels that respond to electrons

Particle - Data Channel	Energy Range	Contaminants
Electron – e1	30 keV to 2500 keV	Proton - 210 keV to 2700 keV
Electron – e2	100 keV to 2500 keV	Proton - 280 keV to 2700 keV
Electron – e3	300 keV to 2500 keV	Proton - 440 keV to 2700 keV
Proton – p6	>6900 keV	Electron – greater than 700 keV

3 Data

We use SEM-2 data from two polar orbiting satellites over 21 years, from 1999 to 2019. The period from the 1st January, 1999 to the 31st December, 2012 and from the 1st January, 2013 to the 31st December, 2019 are covered by the NOAA-15 and the Metop-2 satellite, respectively. NOAA-15 data is available at a 16-second resolution, and Metop-2 data is available at a two-second resolution. The time series representing the relativistic electron flux, namely the p6-90 channel, along with the corresponding L-shell, namely the LGRF parameter, were extracted. Time periods of true solar proton events (SPE) have been excluded by using solar proton activity indications from the P7 omnidirectional detector. This left us with only times during which there are relativistic electron counts in the P6 data channel. Figure 1 shows the electron flux variation with L-shell over past 21 years.

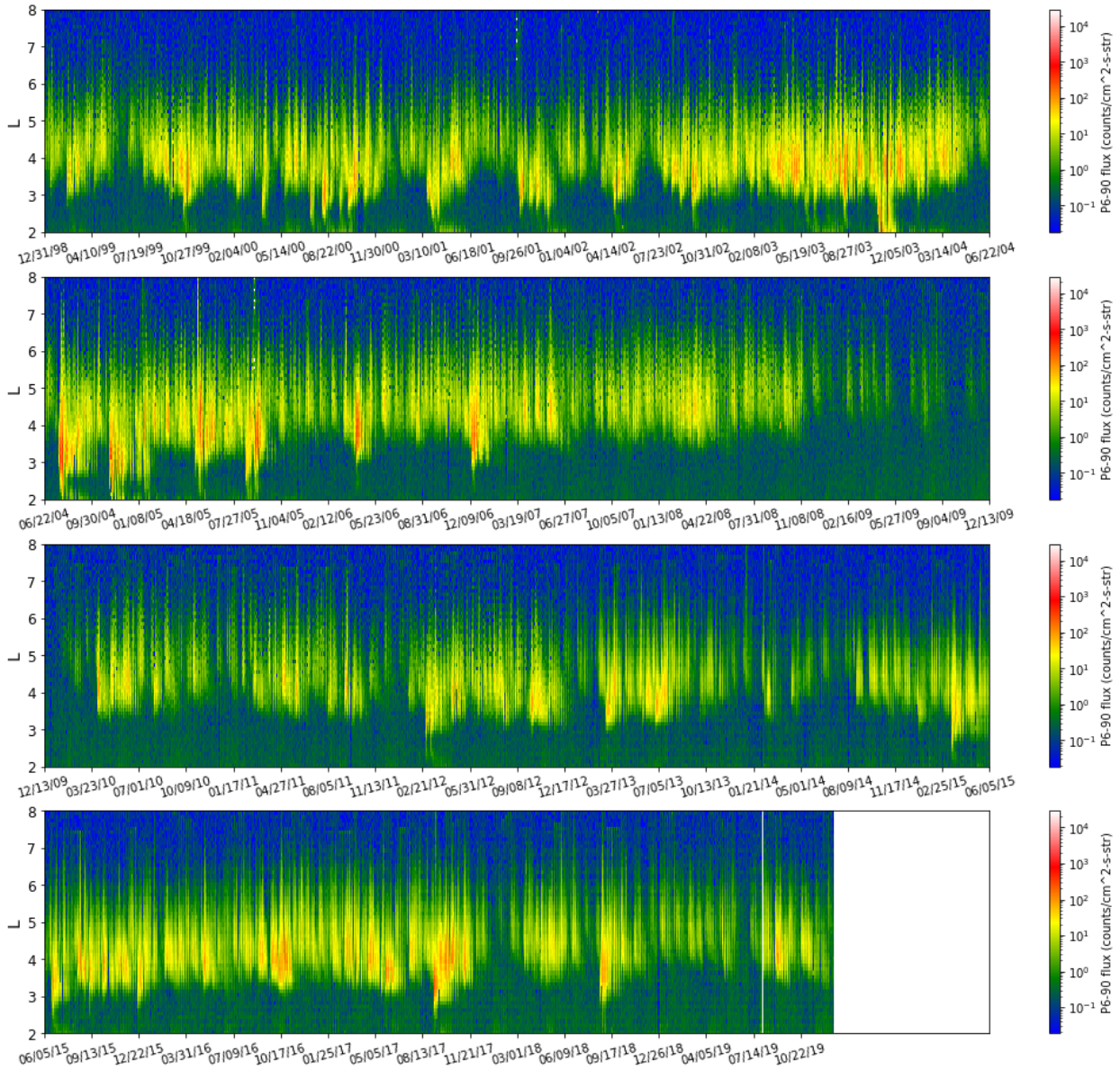

Figure 1. P6-90 electron flux variation with time and L-shell for last 21 years.

Supplementary measurements of one-hour averaged values of solar wind speed, dynamic pressure, electric field and interplanetary magnetic field and geomagnetic indices Dst, Kp and AE were obtained from the NASA OMNI database. ULF indices were obtained from the catalog at http://ulf.gcras.ru/archive.html.

4 Events

Puncture events are identified from the time series of the electron flux in the slot region. The event selection process is described in section 4.1. As events could arise from various physical conditions, we categorize them in section 4.2 before carrying out statistical analysis.

4.1 Event selection

An algorithmic approach is employed for event selection to allow for the varying nature of the puncture events. Our detection algorithm calculates a running average of the electron flux in the region between 2< L<2.8. An event is considered if there is a positive step change in the electron flux by three orders of magnitude. A minimum gap of three days between two events is set to avoid multiple detection. All events detected during an SPE are ignored. A few examples of events are shown in Figure 2.

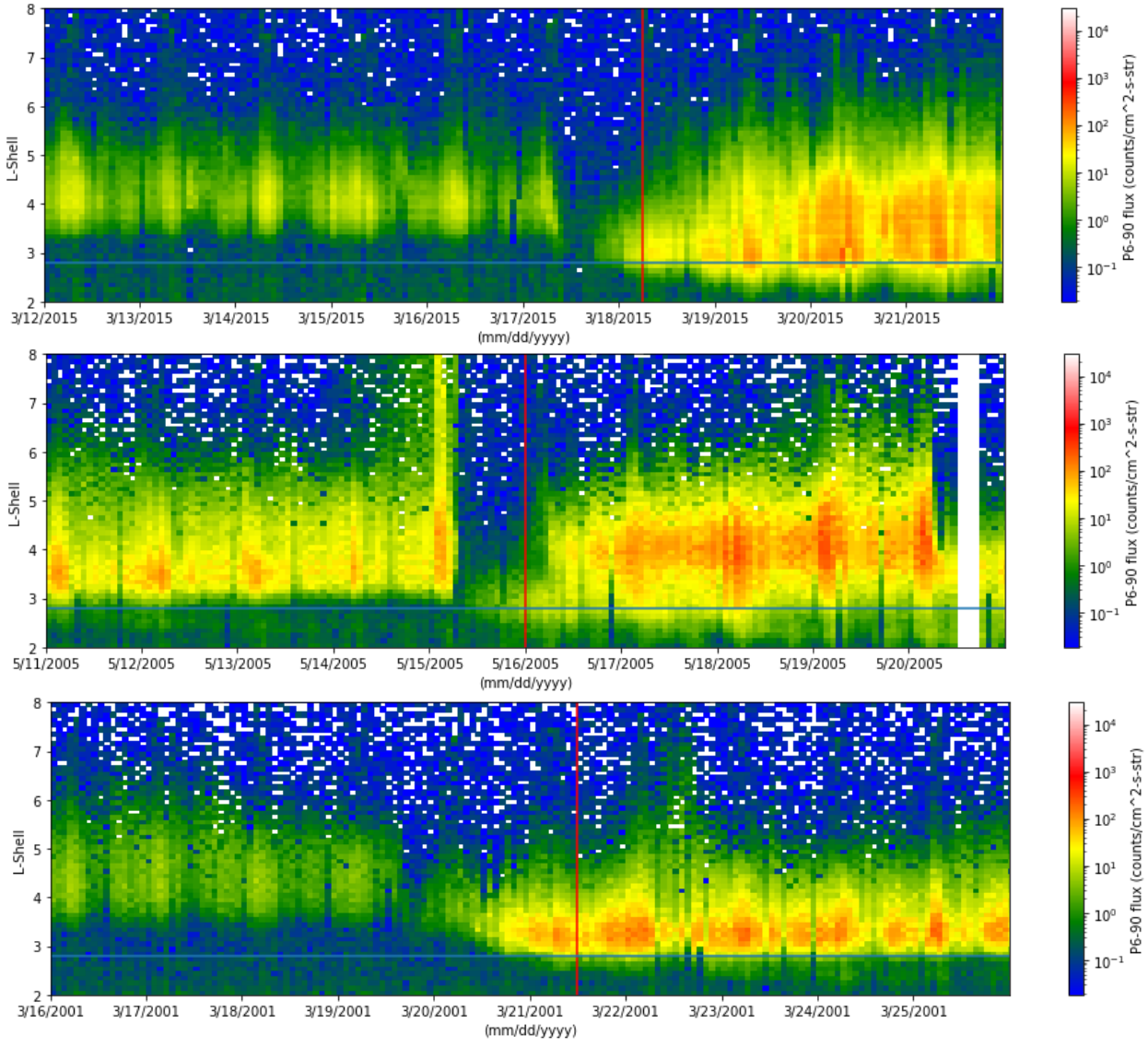

Figure 2. Examples of event detection (red vertical lines). SPE regions are blanked out (white vertical stripes).

The algorithm detected 45 events. Events occurring either overlapping SPE events or within a few hours to SPE events were manually removed. We selected 19 events, which involved only relativistic electrons, for our analysis as shown in Figure 3. It must be noted that some of the puncture events, which were discarded to avoid data ambiguity, could have been true punctures.

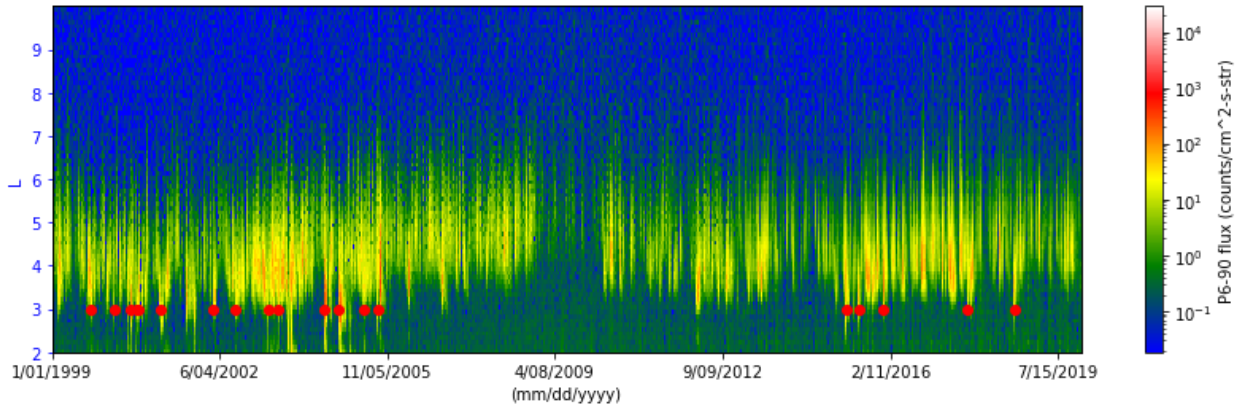

Figure 3. The relativistic electron flux density over 21 years. Selected puncture events are denoted by red dots.

4.2 Event category

A sudden flux increase of relativistic electrons in the slot region is a necessary condition for a puncture event. Radiation belt electron flux variations occur during solar storms, which are caused by either high-speed solar wind-streams (HSSWS) or interplanetary coronal mass ejections (ICMEs) (Friedel et al., 2002). While ICMEs are the main source of geomagnetic storms during the ascending phase of the solar cycle and solar maximum, high-speed (>500 km/s) solar wind-streams play a significant role in the declining phase and solar minimum (Richardson et al., 2000). To reflect the differences in the underlying mechanisms that cause electron puncture events, we break down our data into two categories, which correspond to the ascending and the descending phases of the solar cycle. Average sunspot number is used to determine the phase of the solar cycle.

The condition for breaching the barrier may also depend on the position of the belt's lower boundary. During solar cycle 23 the radiation belt was closer to the earth compared to solar cycle 24 as shown in figure 4.

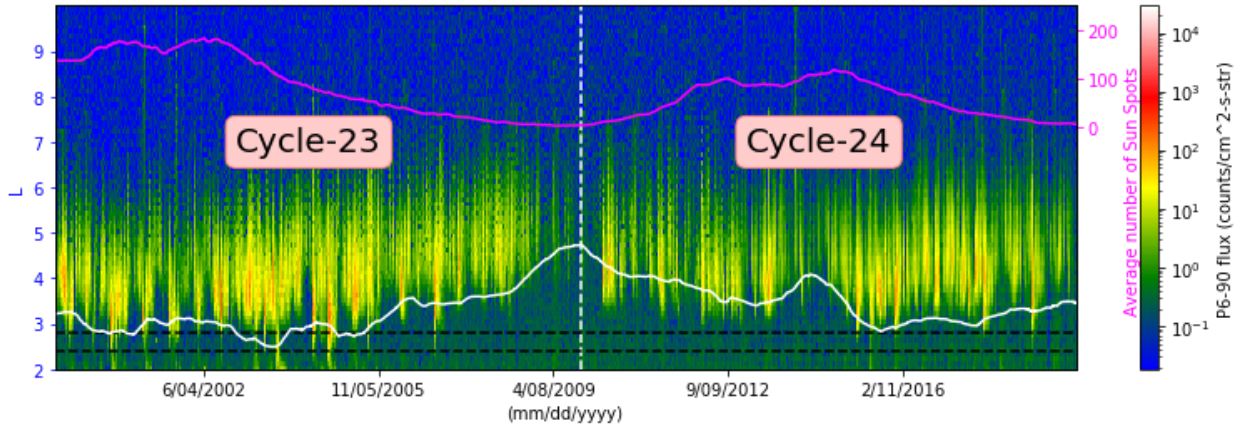

Figure 4. Long-term variation of the lower boundary of the outer radiation belt (white trace) with averaged sunspot numbers (magenta trace).

To account for this cycle-to-cycle variation, we further divide the data into subcategories as ascending-23, descending-23, ascending-24 and descending-24 for solar cycles 23 and 24, as shown in Figure 5. Both ascending-23 and descending-23 categories have seven suitable events each and the descending-24 category has five events. There are no unambiguous puncture events in the ascending-24 category.

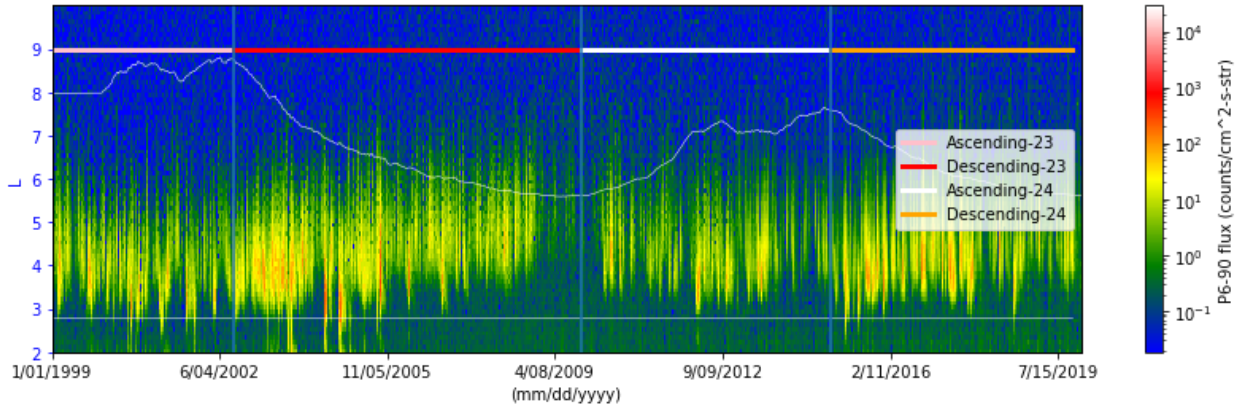

Figure 5. Solar cycle zones to categorize events. Top white trace is the averaged sunspot numbers.

5 Analysis

In this study, we conduct a two-fold analysis of the puncture events. Firstly, we look at various solar indices and solar/magnetospheric parameters around the events. Results of the statistical analysis are presented in section 5.1. Secondly, we examine the ULF wave activity over the study period of 21 years. We then suggest an algorithm that determines the occurrence of punctures, based on this ULF activity. A description of the algorithm and the results are presented in section 5.2.

5.1 Superposed Epoch Analysis

In this analysis, the puncture event time, which is determined by the event selection algorithm (section 4.1), is defined as the 0-epoch. A window of 14 days centered around the event is used in the analysis. Figure 6 and Figure 7 show the superposed epoch analysis of various solar wind parameters and indices. The left panels and the right panels of Figure 6 are the results during the descending-23 and the descending-24 category respectively.

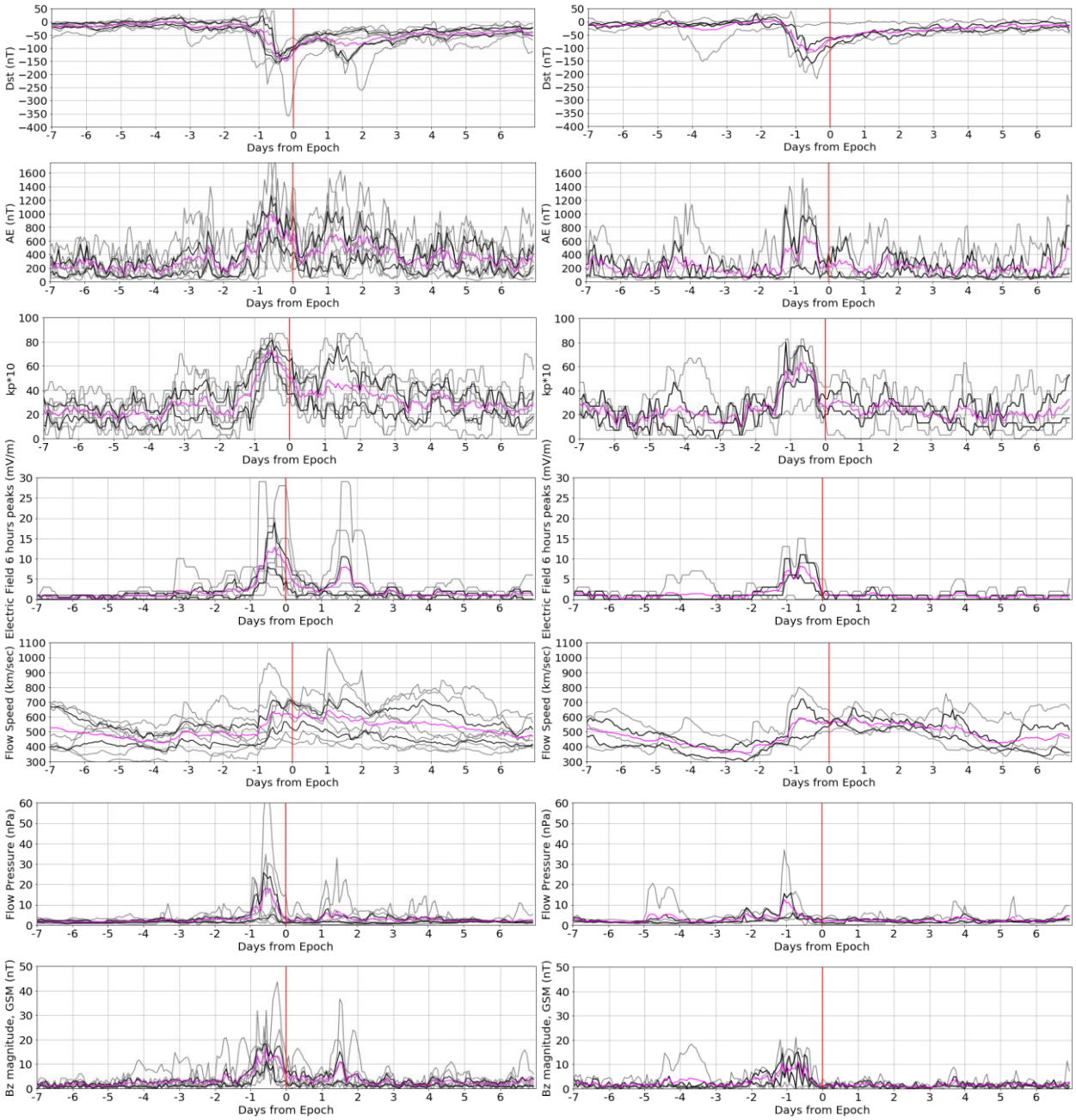

Figure 6. Superposed epoch analysis - left panel and right panel represent solar parameters in descending-23 and descending-24 category respectively. Solar parameters variation (gray lines), mean value (magenta lines), 25th and 75th quartile values (black lines) around the puncture events.

The superposed epoch analysis of descending-23 and ascending-23 categories are shown in Figure 7.

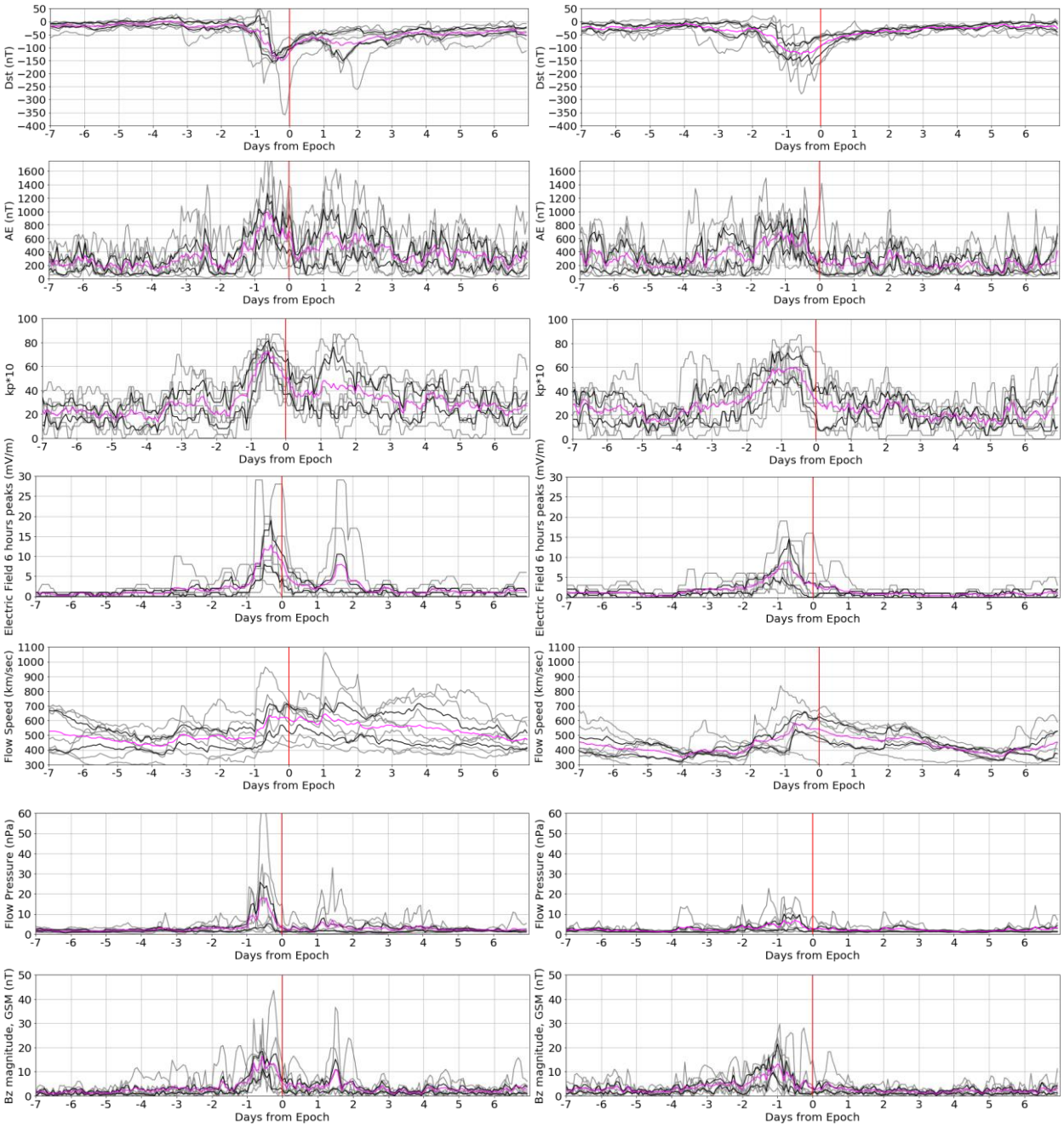

Figure 7. Superposed epoch analysis - left panel and right panel represent solar parameters in descending-23 and ascending-23 category respectively. Solar parameters variation (gray lines), mean value (magenta lines), 25th and 75th quartile values (black lines) around the puncture events.

5.2 ULF Wave Analysis and Puncture Prediction

In this analysis we estimate the enhancement of the energetic electrons in the slot region from the ULF wave activity. Our algorithm uses the ULF indices from the database at http://ulf.gcras.ru/archive.html as a proxy for the strength of ULF signals. From the database we extract two indices, namely the ULF-ground and the ULF-goes. ULF-ground was obtained from the world-wide array of magnetic stations in the Northern hemisphere. ULF-goes was derived from the magnetometers onboard GOES spacecraft. Our prediction algorithm scans the hourly ULF-ground index to identify large disturbances (>200 nT) at very low L-shell. Then the algorithm searches for corresponding disturbances at the geostationary orbit using the ULF-goes index, which reflects the ULF activity at L=6.6. At the geostationary orbit a magnetic disturbance greater than 10 nT is considered significant. We intuit ULF activity in the slot region if a large ULF event occurs simultaneously at the ULF-ground and ULF-goes. The strength of the ULF waves at the geostationary orbit and on the ground, which surround the slot region, is used to predict the puncture events. Figure 8 shows the predicted puncture events in magenta and the identified puncture events in red dots. It should be noted that we discarded many potential puncture events to avoid ambiguity in the input data.

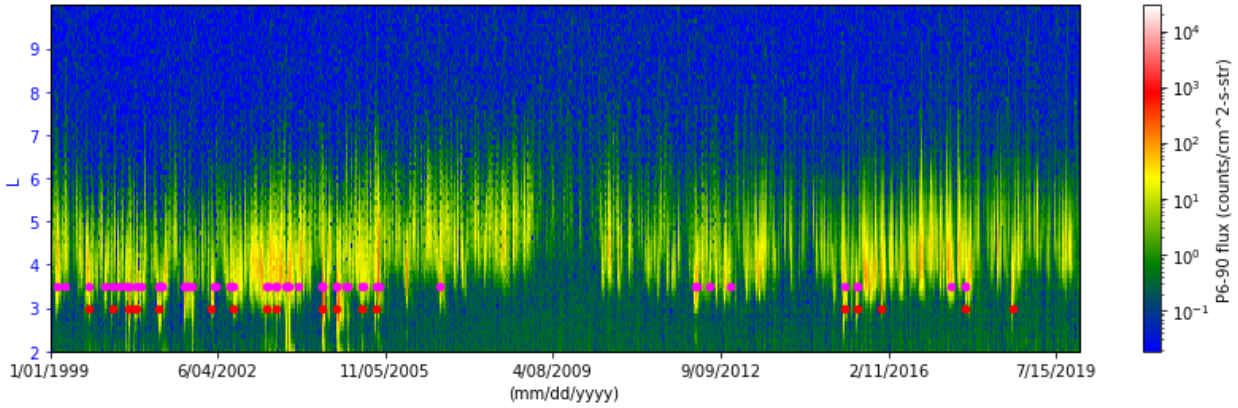

Figure 8. The relativistic electron flux density over 21 years. Puncture events are shown as red dots and predicted events are shown as magenta dots.

6 Discussion and Conclusions

In Figure 6, the solar/magnetospheric parameters are consistently smaller in the right panel representing the descending-24 compared to the left panel representing descending-23. This indicates that the puncture events have no direct correlation with the strength of the geomagnetic activity. Punctures can occur even during a relatively weak solar cycle.

From the fifth row in Figure 7 it can be noted that in the descending-23 category (left panel), the solar wind speed rises over a day and then declines more slowly over several days as compared to the ascending-23 category (right panel). It can also be noted that in the left panels all geomagnetic activities persist for many days as oppose to the right panels where the disturbances are likely caused by ICME. ICME events are more transient, driving high geomagnetic activity for typically only 1–2 days (Richardson et al., 2000).

Approximately 75% of the puncture events could be predicted by our algorithm (Figure 8). The ULF indices database that we used did not include the magnetic stations located in the southern hemisphere. Moreover, we can investigate additional puncture events that were predicted by our algorithm, but were not included as punctures in this study, possibly due to our event detection limitations. All the punctures that occurred during or adjacent to SPE were ignored to avoid the proton contamination in the detector. Careful study of individual events may be necessary to consider those that were left out of this statistical picture.

Energetic electrons can breach the energy-dependent barrier and transit the slot region on occasion, during both ICME and HSS solar driving events. There is no correlation of these puncture events with storm strength or overall geomagnetic activity, however, there exists a strong correlation with ULF wave activity. This study shows the importance of ULF waves in energetic electron enhancements that cause punctures, and, in most cases, it is possible to have a warning.

Acknowledgments and Data

The primary author wishes to acknowledge the use of funds from NASA's Van Allen Probes ECT project, through JHU/APL contract 967399 under prime NASA contract NAS5-01072. NOAA-15 data is available from https://satdat.ngdc.noaa.gov/sem/poes/data/processed/swpc/uncorrected/avg/cdf/ (http://mag.gmu.edu/ftp/POES/n15/). Metop-2 data is available from https://spdf.gsfc.nasa.gov/pub/data/noaa/metop2/sem2_fluxes-2sec/. Solar wind OMNI data is available from https://omniweb.gsfc.nasa.gov/form/dx1.html. ULF wave activity indices are available from ULF wave index database - ESDB repository, GC RAS, Moscow, https://doi.org/10.2205/ULF-index (http://ulf.gcras.ru/archive.html).

References

Baker, D. N., X. Li, J. B. Blake, and S. Kanekal (1998), Strong electron acceleration in the Earth's magnetosphere, *Adv. Space Res.*, 21, 609, doi:10.1016/S0273-1177(97)00970-8.

Baker, D. N., et al. (2014), An impenetrable barrier to ultrarelativistic electrons in the Van Allen radiation belts, *Nature*, 515, 531– 534, doi:10.1038/nature13956.

Blake, J. B., W. A. Kolasinski, R. W. Fillius, and E. G. Mullen (1992), Injection of electrons and protons with energies of tens of MeV into L less than 3 on 24 March 1991, *Geophys. Res. Lett.*, 19, 821–824, doi:10.1029/92GL00624

Friedel, R. H. W., G. D. Reeves, and T. Obara (2002), Relativistic electron dynamics in the inner magnetosphere—A review, *J. Atmos. Sol. Terr. Phys.*, 64, 265, doi:10.1016/S1364-6826(01)00088-8.

Kanekal, S. G., Baker, D. N., & Blake, J. B. (2001), Multisatellite measurements of relativistic electrons: *Global coherence, Journal of Geophysical Research: Space Physics*, 106(A12), 29721-29732, doi: 10.1029/2001JA000070.

Kanekal, S. G. (2006), A review of recent observations of relativistic electron energization in the Earth's outer Van Allen radiation belt, *Proceedings of the ILWS Workshop on Solar Influence on the Heliosphere and Earth's Environment, Goa, India*, Quest Publications, Goa

Li, X., et al. (1993), Simulation of the prompt energization and transport of radiation belt particles during the March 24, 1991 SSC, *Geophysical Research Letters*, 20, Issue 22, doi:10.1029/93GL02701.

Li, X., A. B. Barker, D. N. Baker, W. C. Tu, T. E. Sarris, R. S. Selesnick, R. Friedel, and C. Shen (2009), Modeling the deep penetration of outer belt electrons during the ''Halloween'' magnetic storm in 2003, *Space Weather*, 7, S02004, doi:10.1029/ 2008SW000418.

Liu, W. W., G. Rostoker, D. N. Baker (1999), Internal acceleration of relativistic electrons by large-amplitude ULF pulsations, *J. Geophys. Res. Space Physics*,104, Issue A8, doi:10.1029/1999JA900168.

O'Brien, T. P., et al. (2001), Which magnetic storms produce relativistic electrons at geosynchronous orbit?, *J. Geophys. Res*, 106, NO. A8, 15,533-15,54, doi:10.1029/2001JA000052.

Pilipenko, V., O. Kozyreva, M. Engebretson (2017), ULF wave index database, *ESDB repository, GC RAS*, Moscow, doi:10.2205/ULF-index.

Richardson, I. G., E. W. Cliver, and H. V. Cane (2000), Sources of geomagnetic activity over the solar cycle: Relative importance of CMEs, high-speed streams, and slow solar wind, *J. Geophys. Res.*, 105, 18,203, doi:10.1029/1999JA000400.

Rodger, C. J., M. A. Clilverd, J. C. Green, and M. M. Lam (2010), Use of POES SEM-2 observations to examine radiation belt dynamics and energetic electron precipitation into the atmosphere, *J. Geophys. Res*., 115, A04202, doi:10.1029/2008JA014023.

Rostoker, G., S. Skone, and D. N. Baker (1998), On the origin of relativistic electrons in the magnetosphere, *Geophys. Res. Lett.*, 25, 3701-3704, doi:10.1029/98GL02801.

Selesnick, R. S. (2015), Measurement of inner radiation belt electrons with kinetic energy above 1 MeV, *J. Geophys. Res. Space Physics*, 120, 8339–8349, doi:10.1002/2015JA021387.

Turner, D. L., et al. (2017), Investigating the source of near-relativistic and relativistic electrons in Earth's inner radiation belt, *J. Geophys. Res. Space Physics*, 122, 695–710, doi:10.1002/2016JA023600.

Zhao, H., and X. Li (2013), Inward shift of outer radiation belt electrons as a function of Dst index and the influence of the solar wind on electron injections into the slot region, *J. Geophys. Res. Space Physics*, 118, 756–764, doi:10.1029/2012JA018179.